

Sulfate Recognition in Water via Charge-Assisted Hydrogen Bonding

Alexander Mariscal,^[a] Luzelena Sagal,^[a] Carson Doan,^[a] Canjia Zhai,^[a] Dexin Liu,^[a] Lukasz Wojtas,^[a] and Wenqi Liu*^[a]

Achieving selective molecular recognition of hydrophilic anions in water remains a formidable challenge due to the competitive nature of water and the high hydration energies of target anions such as sulfate. Here, we report the design, synthesis, and characterization of a simple dicationic tetralactam macrocycle (BPTL²⁺·2Cl⁻) capable of binding highly hydrated anions in water via charge-assisted hydrogen bonding. Structural, spectroscopic, thermodynamic, and computational studies reveal that BPTL²⁺ exhibits a strong binding affinity for sulfate ($K_a = 2892 \text{ M}^{-1}$), driven primarily by entropic gain from water release and reinforced by electrostatic and hydrogen bonding interactions. Single-crystal X-ray diffraction and DFT-optimized

structures confirm the formation of directional [N—H•••O] and [C—H•••O] hydrogen bonds. Comparative studies with a control macrocycle (6Na⁺·HCTL⁶⁻) that has a charge-neutral binding cavity underscore the essential role of cationic charge in overcoming desolvation enthalpic penalties. The receptor displays anti-Hofmeister selectivity, preferentially binding more hydrophilic anions. This work provides fundamental insights into the mechanisms of anion recognition in water. It establishes charge-assisted hydrogen bonding as a powerful strategy for developing next-generation receptors for sensing, separation, sequestration, transport, and catalysis in aqueous environments.

1. Introduction

Developing synthetic receptors capable of recognizing polar and hydrophilic substrates in aqueous environments remains a significant yet unresolved challenge in supramolecular chemistry.^[1–9] Achieving selective and effective binding of such targets in water would unlock a broad range of applications, including chemical sensing,^[10,11] environmental remediation,^[12,13] disease diagnostics,^[14–17] and toxin sequestration.^[18–20] Among these challenging targets, sulfate (SO₄²⁻) is particularly difficult to bind due to its high charge density and exceptionally strong hydration energy (−1103 kJ mol⁻¹), placing it near the hydrophilic end of the Hofmeister series.^[21] From an applied perspective, the sulfate anion poses serious obstacles in nuclear waste management by interfering with vitrification processes and accelerating corrosion in glass melters.^[22,23] Elevated sulfate concentrations in water can lead to ecosystem imbalance, corrosion of infrastructure, and increased treatment costs due to scaling and reduced efficiency in industrial and desalination systems.^[24,25] Despite its practical importance, there remains a fundamental gap in our understanding of how to rationally design and synthesize molecular receptors that can effectively bind sulfate in water. Developing sulfate-binding receptors could offer novel solutions for improving nuclear waste processing and reduc-

ing environmental and industrial impacts by mitigating scaling, corrosion, and sulfate pollution in industrial and desalination systems.

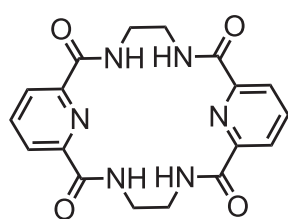
Most studies on anion binding with synthetic receptors have been performed in organic solvents, where hydrogen bonding is more effectively utilized.^[26–38] Conversely, achieving effective molecular recognition of hydrophilic anions in water through hydrogen bonding presents a significant challenge. This issue primarily arises from water's unique properties—it serves as a highly competitive hydrogen-bonding medium, acting both as a donor and an acceptor. In aqueous environments, the hydrogen-bond donor sites on synthetic hosts often face competition from solvent molecules. Additionally, the high polarity of water reduces the strength of noncovalent interactions like hydrogen bonds and electrostatic attractions, subsequently lowering receptor–substrate affinity. Furthermore, the strong solvation of polar functional groups in water introduces a considerable desolvation energy barrier that must be overcome during binding.^[2,5,9,39–42]

Despite these obstacles, a limited number of hydrogen bonding receptors have demonstrated sulfate recognition in water. Noteworthy examples include Kubik's molecular oyster^[43] and Wu's [2.2]urea cryptand,^[44] which exemplify the crucial role of shape complementarity between the binding pocket and the tetrahedral structure of the sulfate anion. Recent work from the Custelcean and White groups^[13,22,45] has shown that incorporating charged functionalities, such as guanidinium and pyridinium, into receptor architectures can help offset sulfate's high hydration energy, enabling effective binding or precipitation in aqueous media. These receptors leverage a synergistic combination of electrostatics and directional hydrogen bonding, giving rise to charge-assisted hydrogen bonding that significantly improves

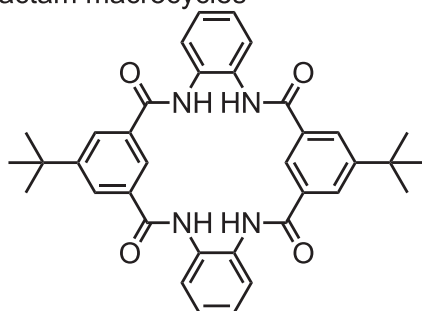
[a] A. Mariscal, L. Sagal, C. Doan, C. Zhai, D. Liu, L. Wojtas, W. Liu
 Department of Chemistry, University of South Florida, 4202 E. Fowler Ave,
 Tampa, Florida 33620, USA
 E-mail: wenqi@usf.edu

Supporting information for this article is available on the WWW under
<https://doi.org/10.1002/chem.202501400>

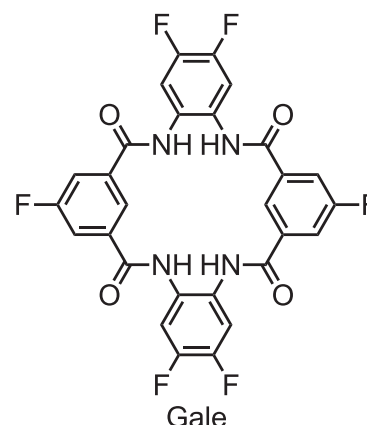
(a) Previously reported tetralactam macrocycles



Jurczak



Smith



Gale

(b) This study

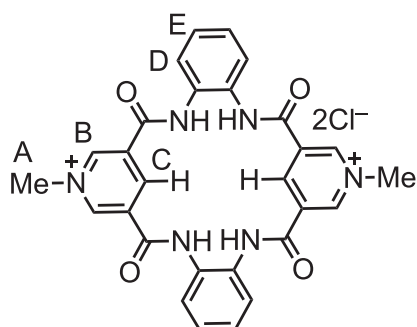
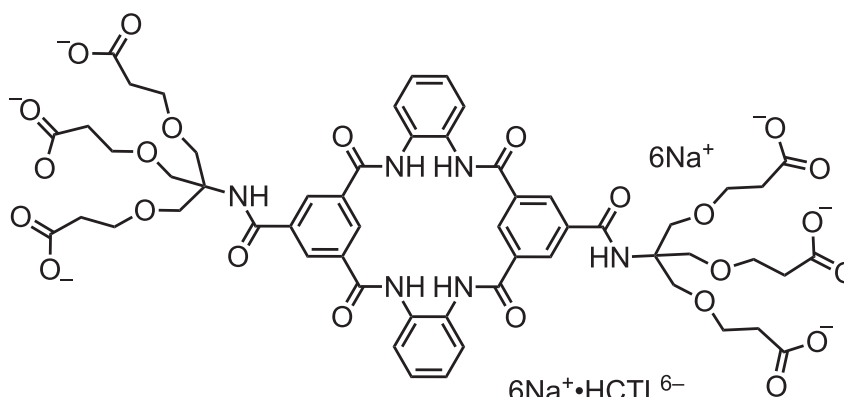
BPTL²⁺•2Cl⁻6Na⁺•HCTL⁶⁻

Figure 1. Structural formulas of (a) previously reported tetralactam macrocycles and (b) hydrogen bonding receptors BPTL²⁺•2Cl⁻ and 6Na⁺•HCTL⁶⁻ investigated in this study.

binding efficacy for highly hydrated anions. Nevertheless, the relative contributions of electrostatic versus hydrogen bonding interactions remain poorly understood, mainly due to a lack of systematic studies to isolate and assess these fundamental noncovalent forces.

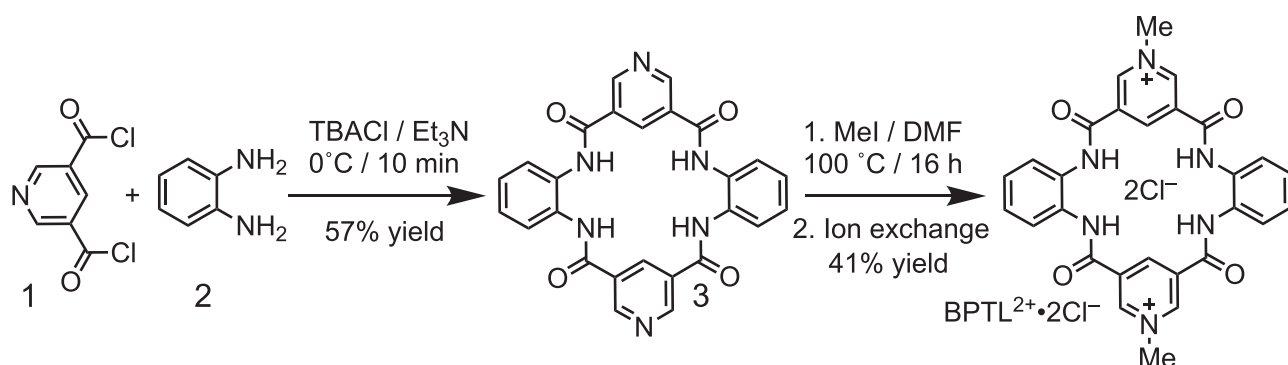
In this study, we aim to dissect the respective roles of charge and hydrogen bonding in the aqueous recognition of hydrophilic anions. Our group previously reported^[46] a pyridinium-functionalized bicyclic cage featuring both charged and hydrogen bonding residues confined within a hydrophobic cavity, where anion binding was influenced by a combination of electrostatics, hydrogen bonding, and hydrophobic effects. To decouple and better understand these contributions, we now turn to simpler receptor architectures that feature charge-assisted hydrogen bonding without a hydrophobic environment. Tetralactam macrocycles, as reported (Figure 1a) by Jurczak,^[47] Smith,^[48] and Gale,^[49] provide an ideal platform. These macrocycles possess simple modular structures with four convergent NH groups forming a shallow binding cavity and have been previously studied for halide binding and transport. However, their potential to bind highly hydrated anions such as sulfate in water has not yet been explored. Their structural simplicity and synthetic accessibility make them ideal candidates for systematically probing the interplay between hydrogen bonding and electrostatics in recognizing hydrophilic anions.

2. Results and Discussion

2.1. Molecular Design Principle

Our newly developed bipyrindinium-based tetralactam macrocycle (BPTL²⁺•2Cl⁻) features (Figure 1b) four convergent amide NH groups, forming a well-defined hydrogen bonding cavity. Incorporating pyridinium units enhances water solubility and introduces two polarized C—H bonds that can serve as additional hydrogen bond donors within the binding pocket.^[46,50,51] Moreover, the positive charges of the pyridinium rings are positioned near the binding cavity, enabling charge-assisted hydrogen bonding and making BPTL²⁺•2Cl⁻ a water-soluble receptor with enhanced anion recognition capabilities.

To unravel the respective contributions of charge and hydrogen bonding in anion recognition, we sought to develop a water-soluble tetralactam macrocycle featuring a charge-neutral binding cavity. Potential solubilization strategies involve either neutral oligoethylene glycol chains or anionic carboxylates. Given the known tendency of oligoethylene glycol-functionalized organic molecules to aggregate in water,^[52] we opted for the latter approach. We designed a hexacarboxylate tetralactam macrocycle (6Na⁺•HCTL⁶⁻) incorporating two carboxylate-bearing dendrons, which provide excellent water solubility while effectively preventing macrocycle aggregation. Given the significant screening of electrostatic interactions in

Scheme 1. Synthesis of BPTL²⁺·2Cl⁻.

aqueous media, the negatively charged carboxylate groups located far from the central binding site should exert minimal influence on the binding event.^[42] This charge-neutral binding pocket, devoid of nearby charge effects, provides a control structure to isolate and evaluate the individual roles of hydrogen bonding and electrostatics in the aqueous recognition of hydrophilic anions.

2.2. Synthesis

BPTL²⁺·2Cl⁻ was readily synthesized (Scheme 1) in two steps. The key intermediate, tetralactam macrocycle 3, was obtained in a good yield of 57% by reacting acyl chloride 1 with benzene-1,2-diamine 2 in the presence of Et₃N as a base and tetrabutylammonium chloride (TBACl) as a templating agent. The template was easily removed by simple solvent washing. Subsequent *N*-alkylation of macrocycle 3 with iodomethane, followed by a standard ion exchange procedure, afforded the water-soluble receptor BPTL²⁺·2Cl⁻. The control molecule 6Na⁺·HCTL⁶⁻ was prepared following the reported procedure.^[48]

2.3. Structural Analysis by Single-Crystal X-ray Diffraction

Single crystals of the chloride-bound tetralactam macrocycle (Cl⁻⊂3) were obtained via slow diffusion of pentane into a CHCl₃ solution containing tetralactam macrocycle 3 and TBACl. The X-ray crystal structure (Figure 2a,b) reveals that the macrocycle adopts a saddle-shaped conformation with a torsion angle of 11° between the phenyl and pyridine rings. The central cavity is formed by four convergent N—H hydrogen bond donors and two polarized C—H bonds, creating a shallow but well-defined binding site. The encapsulated chloride anion is located above the center of the macrocycle and stabilized by six hydrogen bonds. The [N···Cl] distances range from 3.34 to 3.37 Å, with [N—H···Cl] bond angles of 169.1° to 170.7°, indicative of moderate-strength hydrogen bonding.

Similarly, single crystals of the acetate-bound macrocycle (AcO⁻⊂3) were obtained by slow diffusion of pentane into a solution containing macrocycle 3 and tetrabutylammonium acetate (TBAOAc). The macrocycle retains (Figure 2c) a saddle-shaped conformation with an increased torsion angle of 29°

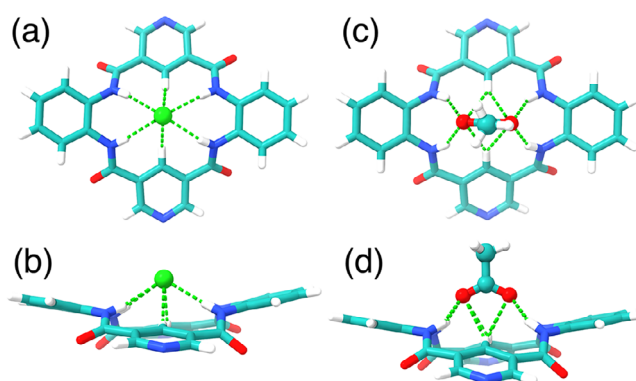


Figure 2. (a) Front and (b) side-on view of X-ray single crystal structure of Cl⁻⊂tetralactam macrocycle 3. (c) Front and (d) side-on view of X-ray single crystal structure of AcO⁻⊂tetralactam macrocycle 3. The green dashed line represents hydrogen bonds.

between the phenyl and pyridine rings. The acetate anion is positioned (Figure 2d) perpendicular to the macrocycle plane, with its carboxylate group engaged in hydrogen bonding with four N—H and two C—H donors. The [N···O] distances range from 2.73 to 2.75 Å, and the [N—H···O] bond angles fall between 151.8° and 151.9°, again suggesting moderate hydrogen bonding strength.

2.4. Anion Binding Study in Water by NMR Spectroscopy and ITC

Proton nuclear magnetic resonance (¹H NMR) spectroscopy was employed to investigate the anion-binding behavior of BPTL²⁺·2Cl⁻ in aqueous solution. To directly probe the hydrogen bonding interactions between BPTL²⁺·2Cl⁻ and SO₄²⁻, measurements were initially conducted in a 10% D₂O / 90% H₂O solvent mixture. However, the amide N—H signals were not observable under these conditions due to rapid D/H exchange. A small amount of HCl (1 mM) was added to the solution to suppress this exchange and enable monitoring of N—H resonances. After SO₄²⁻ (5 mM) was added, distinct downfield shifts were observed (Figure 3a) for both the amide N—H and the aromatic C—H protons that orient toward the central binding cavity. These chemical shift changes provide compelling evidence that BPTL²⁺·2Cl⁻ engages in hydrogen bonding with SO₄²⁻ in water.

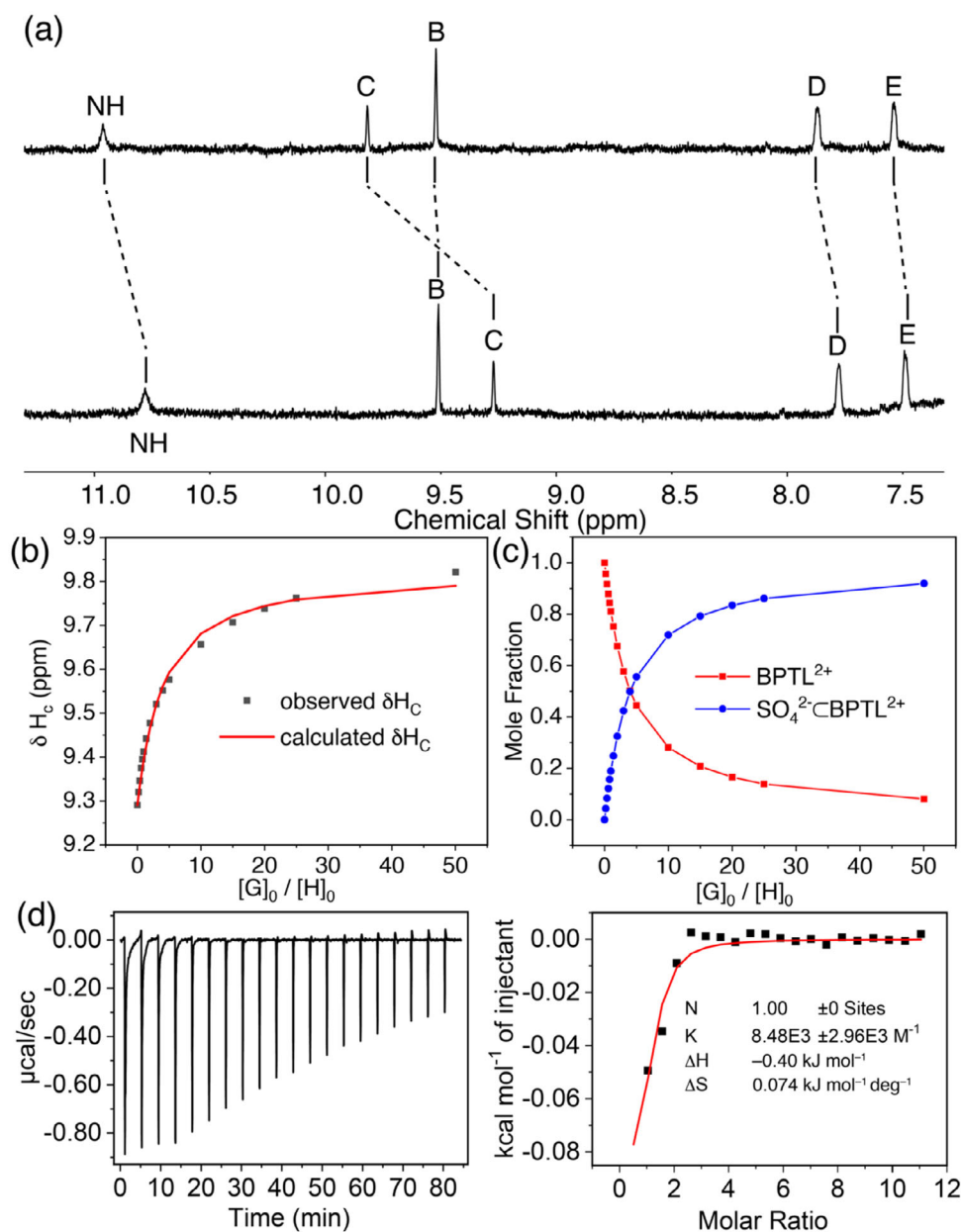


Figure 3. (a) ¹H NMR spectra (600 MHz, 10% D₂O / 90% H₂O) of solutions containing BPTL²⁺·2Cl⁻ (0.1 mM) with only (bottom) HCl (1 mM) and (top) with HCl (1 mM) plus Na₂SO₄ (5 mM). Proton labels are displayed in Figure 1. (b) Nonlinear fitting of the chemical shift changes of proton C during the titration of BPTL²⁺·2Cl⁻ with Na₂SO₄ in D₂O. (c) Calculated mole fraction changes of free BPTL²⁺ and the sulfate complex (SO₄²⁻·BPTL²⁺) in D₂O as a function of the guest–host mole ratio. (d) ITC profile of BPTL²⁺·2Cl⁻ (0.8 mM) during titration with Na₂SO₄.

To evaluate the anion-binding affinity of BPTL²⁺·2Cl⁻ in water, separate ¹H NMR titration experiments were performed in D₂O without the addition of HCl or H₂O. Among the observed resonances, the most pronounced chemical shift changes occurred for proton C, which is oriented toward the binding cavity and thus highly sensitive to anion interactions. Consequently, the chemical shift changes of proton C were used for nonlinear curve fitting (Figure 3b) to determine binding constants. Under the titration conditions, approximately 80% of BPTL²⁺·2Cl⁻ (0.1 mM) became saturated when the concentration of SO₄²⁻ exceeded 2 mM (Figure 3c). Nonlinear fitting of the titra-

tion data yielded^[53,54] a binding constant of (2892 ± 322) M⁻¹, indicating a strong affinity of BPTL²⁺·2Cl⁻ for SO₄²⁻ in water.

Table 1 summarizes the binding constants of BPTL²⁺·2Cl⁻ with various anions in aqueous solution. The dianionic oxalate exhibited a moderate binding affinity of 887 M⁻¹ among the tested species. In contrast, acetate—despite its structural similarity—showed a tenfold weaker affinity of 87 M⁻¹. All tested anions carrying a single negative charge displayed significantly lower binding affinities, generally below 100 M⁻¹. These observations suggest that electrostatic interactions play a dominant role in the binding behavior of BPTL²⁺·2Cl⁻.

Table 1. A summary of association constants and thermodynamic parameters for 1:1 complexes of BPTL²⁺·2Cl⁻ and 6Na⁺·HCTL⁶⁻ with anions in D₂O or H₂O as determined by ¹H NMR titrations and ITC at 23 °C.

| Guest ^[a] | BPTL ²⁺ /K _a (M ⁻¹) | | ΔG ^{d]} kJ mol ⁻¹ | ΔH ^{d]} kJ mol ⁻¹ | TΔS ^{d]} kJ mol ⁻¹ | HCTL ⁶⁻ NMR |
|---|---|---------------------|--|--|---|---------------------------|
| | NMR | ITC ^[d] | | | | |
| SO ₄ ²⁻ | 2892 ± 322 | 8480 ± 2960 | -22.3 | -0.4 | 21.9 | N.B. ^[b] |
| C ₂ O ₄ ²⁻ | 887 ± 66 | N.D. ^[c] | N.D. ^[c] | N.D. ^[c] | N.D. ^[c] | N.B. ^[b] |
| AcO ⁻ | 87 ± 2 | 68 ± 10 | -10.7 | +5.6 | 16.3 | N.B. ^[b] |
| Cl ⁻ | 88 ± 7 | 47 ± 6 | -9.6 | -4.6 | 5.0 | N.B. ^[b] |
| Br ⁻ | 52 ± 11 | 54 ± 18 | -9.6 | -2.5 | 7.1 | N.B. ^[b] |
| I ⁻ | 85 ± 11 | 28 ± 5 | -8.4 | -4.2 | 4.2 | N.B. ^[b] |
| NO ₃ ⁻ | N.B. ^[b] | N.D. ^[c] | N.D. ^[c] | N.D. ^[c] | N.D. ^[c] | N.B. ^[b] |
| ClO ₄ ⁻ | N.B. ^[b] | N.D. ^[c] | N.D. ^[c] | N.D. ^[c] | N.D. ^[c] | N.B. ^[b] |

^[a] All anion titrations were performed using their corresponding sodium salts.

^[b] No appreciable binding was detected.

^[c] Not determined due to either lack of measurable binding or a binding enthalpy below the sensitivity limit of our MicroCal ITC.

^[d] Roughly estimated data on account of either low affinity or low heat formation.

Notably, the receptor's binding affinity for its counterion, Cl⁻, was relatively weak at 88 M⁻¹. This implies that at low concentrations (<0.5 mM), over 90% of BPTL²⁺ remains unbound, with Cl⁻ dissociating from the binding pocket. Thus, the influence of Cl⁻ on measured binding affinities under these conditions is minimal. Br⁻ and I⁻ showed similar weak affinities to Cl⁻. Oxyanions such as NO₃⁻ and ClO₄⁻ exhibited no measurable binding, consistent with their position at the hydrophobic end of the Hofmeister series. Their inability to participate in strong hydrogen bonding or electrostatic interactions with BPTL²⁺ likely accounts for this lack of binding. Overall, BPTL²⁺·2Cl⁻ demonstrates an anti-Hofmeister selectivity pattern, preferentially binding more hydrophilic anions in water—a behavior rarely observed in aqueous anion receptors.^[55–58]

In comparison, the control molecule 6Na⁺·HCTL⁶⁻ equipped with a charge-neutral binding pocket showed no appreciable binding to any tested anions under similar conditions. This result highlights the intrinsic difficulty of achieving effective anion recognition in water using hydrogen bonding alone.^[42] These findings underscore that anion binding by BPTL²⁺ in water is governed by a combination of electrostatic attraction, hydrogen bonding, and size complementarity with the binding cavity. Charge-assisted hydrogen bonding thus emerges as a powerful strategy for recognizing hydrophilic anions in aqueous environments.

Isothermal titration calorimetry (ITC) was employed to investigate the thermodynamic driving forces underlying the anion binding affinities and selectivities observed for BPTL²⁺·2Cl⁻. The binding affinities determined by ITC generally followed the same trend as those obtained from ¹H NMR titration experiments, though they should be interpreted as approximate values. Accurate determination of binding enthalpies was limited by either the low heat released upon binding or by weak interactions, both of which fall outside the optimal detection range of ITC.

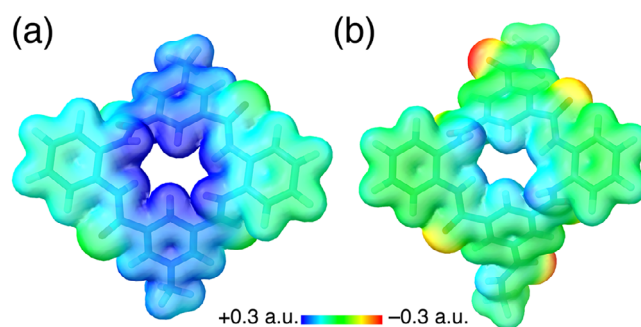


Figure 4. ESP of (a) BPTL²⁺ and (b) truncated HCTL⁶⁻.

Despite these limitations, all anion-binding events were found (Figure 3d) to be primarily entropy-driven.^[59,60] For SO₄²⁻, the enthalpic contributions were minimal, with ΔH values near -0.4 kJ mol⁻¹. This observation suggests that the electrostatic interactions between BPTL²⁺ and the dianionic guest are sufficient to nearly compensate for the enthalpic cost associated with desolvation. The dominant driving force in this case is attributable to the release of bound water molecules from the highly hydrated anions into the bulk solvent, resulting in a favorable entropy gain (TΔS = 21.9 kJ mol⁻¹).

Interestingly, the binding of AcO⁻ displayed a weakly endothermic profile, indicating that the electrostatic interactions between AcO⁻ and BPTL²⁺ are insufficient to overcome the dehydration energy barrier. Nevertheless, the overall process is still driven forward by the entropic benefit of water molecule release, enabling complex formation despite the positive enthalpy change. Binding interactions with halides were characterized by modest enthalpic and entropic contributions, consistent with their weaker binding affinities. These results indicate that the charge-assisted hydrogen bonding exhibited by BPTL²⁺ operates primarily through dehydration-driven mechanisms. The release of structured water molecules from hydrophilic anions plays a central role in driving their recognition and binding in aqueous environments.

2.5. Computational Analysis

Computational modeling was employed to understand detailed structural patterns for the macrocycle and its anion complexes. Structural optimization of BPTL²⁺ and truncated HCTL⁶⁻ was performed by density functional theory at the level of BLYP-D3/SVP. Both structures present binding pockets with convergent NH hydrogen bond donors. On account of the pyridinium residues, the electrostatic potential map (ESP) of BPTL²⁺ presents (Figure 4a) a large area of positively charged isosurface, establishing an electronic field that is ready to accept the anions at the binding pocket. In contrast, the charge-neutral core of HCTL⁶⁻ only shows (Figure 4b) slightly positive regions at the isosurface near N—H residues, which can only attract anions through hydrogen bonding without the benefit of electrostatic attractions.

Conformational isomers of the SO₄²⁻·BPTL²⁺ and C₂O₄²⁻·BPTL²⁺ complexes were initially sampled using the

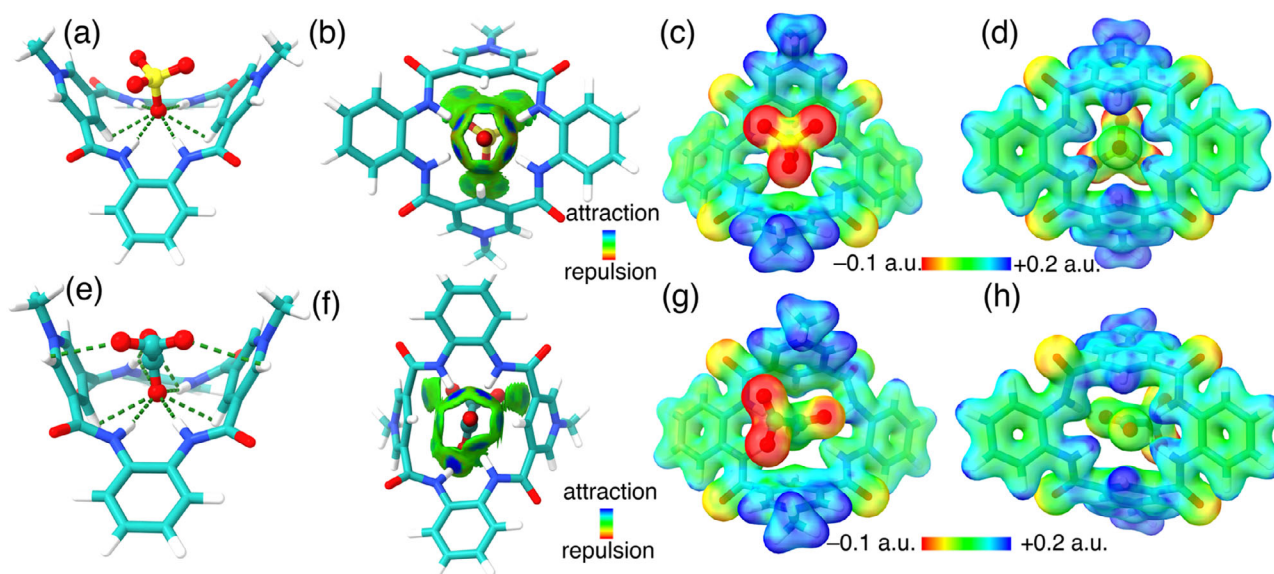


Figure 5. (a) DFT-optimized structure of $\text{SO}_4^{2-}\text{-BPTL}^{2+}$. (b) IGM isosurface representing noncovalent interactions between SO_4^{2-} and BPTL^{2+} . Noncovalent interaction isosurface is displayed at $\delta g^{\text{inter}} = 0.005$ a.u.; color coding in the electron density range of $0.05 < \text{sign}(\lambda_2)\rho < +0.05$ a.u. (c) top view and (d) side-on view of ESP for $\text{SO}_4^{2-}\text{-BPTL}^{2+}$. (e) DFT-optimized structure of $\text{C}_2\text{O}_4^{2-}\text{-BPTL}^{2+}$. (f) IGM isosurface representing noncovalent interactions between $\text{C}_2\text{O}_4^{2-}$ and BPTL^{2+} . Noncovalent interaction isosurface is displayed at $\delta g^{\text{inter}} = 0.005$ a.u.; color coding in the electron density range of $-0.05 < \text{sign}(\lambda_2)\rho < +0.05$ a.u. (g) top view and (h) side-on view of ESP for $\text{C}_2\text{O}_4^{2-}\text{-BPTL}^{2+}$.

CREST program in NCI mode.^[61,62] The lowest-energy candidates were then further optimized by DFT at the BLYP-D3/SVP level to identify the likely global minimum structures. In the optimized structure of $\text{SO}_4^{2-}\text{-BPTL}^{2+}$, one oxygen atom from the SO_4^{2-} anion participates (Figure 5a) in hydrogen bonding interactions. This oxygen atom engages in four [N—H•••O] hydrogen bonds and two additional [C—H•••O] interactions involving the inward-facing para C—H bonds on the pyridinium rings. The [N—H•••O] bond distances range from 1.97 to 2.00 Å, with corresponding bond angles between 173° and 175°, indicative of strong, directional hydrogen bonding. Meanwhile, the remaining three oxygen atoms of the SO_4^{2-} point toward the pyridinium nitrogens, establishing electrostatic attractions.

An independent gradient model (IGM) analysis^[63–65] was performed to further visualize these noncovalent interactions. The IGM isosurfaces, color-coded to represent interaction strength, clearly reveal (Figure 5b) an isosurface encircling the oxygen atom, corresponding to four [N—H•••O] and two [C—H•••O] interactions. Notably, the SO_4^{2-} oxygen is associated with darker blue isosurfaces for [N—H•••O] interactions compared to the [C—H•••O] interactions, indicating that the NH groups participate in stronger hydrogen bonding than the CH groups. Additionally, three distinctive isosurfaces were revealed between the remaining oxygens of the SO_4^{2-} and the pyridinium panels, highlighting regions involved in long-range electrostatic attractions. This analysis provides compelling visual evidence of the charge-assisted hydrogen bonding interactions that stabilize the sulfate complex.

Atom dipole-corrected Hirshfeld charge analysis^[66] of the $\text{SO}_4^{2-}\text{-BPTL}^{2+}$ complex reveals that the oxygen atom of SO_4^{2-} engaged in hydrogen bonding with the macrocycle possesses partial charges of -0.33 . In contrast, the remaining three oxygen

atoms, oriented toward the pyridinium rings, exhibit nearly identical charges of -0.51 . These results indicate that charge-assisted hydrogen bonding effectively stabilizes SO_4^{2-} within the binding pocket and partially neutralizes its negative charges. This conclusion is further supported by the electrostatic potential (ESP) maps of the $\text{SO}_4^{2-}\text{-BPTL}^{2+}$ complex (Figure 5c,d), which show^[67] the electronegative SO_4^{2-} anion enveloped by the electropositive BPTL^{2+} host. Notably, both the binding cavity and the hydrogen-bonded oxygen atom of SO_4^{2-} exhibit green-coded isosurfaces at the contact regions, corresponding to areas of near-zero electrostatic potential, signifying mutual electrostatic compensation at these interaction sites.

In the optimized structure of the $\text{C}_2\text{O}_4^{2-}\text{-BPTL}^{2+}$ complex, one of the two carboxylate groups is positioned within the binding cavity and actively participates in hydrogen bonding. This carboxylate group is oriented (Figure 5e) toward the phenyl ring, a binding orientation that closely resembles the arrangement observed in the single-crystal structure of the $\text{AcO}^-\text{-tetralactam}$ macrocycle 3 complex. Within the cavity, three NH groups point toward one carbonyl oxygen and one NH group point toward the remaining oxygen of the carboxylate group in the binding pocket, forms four strong hydrogen bonds with amide residues, with [N—H•••O] bond distances of 1.90, 1.87, 2.15, and 1.83 Å, and corresponding bond angles of 167°, 176°, 160°, and 170°, respectively, consistent with strong and highly directional hydrogen bonding. The other carboxylate group of oxalate is in an orthogonal position and oriented toward the pyridinium rings, establishing electrostatic attraction and [C—H•••O] hydrogen bonds.

IGM analysis provided (Figure 5f) detailed insights into the noncovalent interactions present in the $\text{C}_2\text{O}_4^{2-}\text{-BPTL}^{2+}$ complex. The four strong [N—H•••O] hydrogen bonds between the

carboxylate group and the amide residues are visualized as distinct dark blue isosurfaces, indicating strong and directional interactions. In addition, multiple isosurfaces corresponding to [C—H...O] interactions were observed for both carboxylate groups, highlighting the additional stabilizing contributions from these weaker hydrogen bonds. Atom dipole-corrected Hirshfeld charge analysis was performed to further probe the electronic environment. The two oxygen atoms on the carboxylate group located within the binding cavity exhibited partial charges of -0.40 and -0.33 , whereas the oxygens on the unbound carboxylate group carried equal negative charges of -0.53 . This disparity suggests that the carboxylate group engaged in binding undergoes partial charge neutralization as a result of charge-assisted hydrogen bonding with the macrocycle. This conclusion is further supported (Figure 5g,h) by ESP calculations, which show a clear reduction in electron density on the oxygen atoms involved in hydrogen bonding.

Together, these computational results underscore the distinct roles of charge and hydrogen bonding in anion binding by BPTL²⁺. While both BPTL²⁺ and HCTL⁶⁻ feature convergent hydrogen bond donors, only BPTL²⁺ provides a strongly electropositive cavity that amplifies binding through charge-assisted hydrogen bonding. Detailed analyses of the SO₄²⁻ and C₂O₄²⁻ complexes reveal robust networks of directional [N—H...O] and auxiliary [C—H...O] interactions, visualized by IGM surfaces and quantified by Hirshfeld charge shifts. These findings confirm that electrostatic complementarity and charge compensation at the binding interface are pivotal for stabilizing anionic guests, highlighting the synergy between hydrogen bonding and electrostatic effects in aqueous anion recognition.

3. Conclusion

We have investigated the anion-binding properties of a simple dicationic tetralactam macrocycle in aqueous solution. Our findings highlight the critical role of receptor charges in restoring and enhancing hydrogen bonding capability in water. Specifically, charge-assisted hydrogen bonding enables adequate compensation for the substantial enthalpic cost associated with the dehydration of the highly hydrophilic SO₄²⁻ anion. Simultaneously, dehydration provides a favorable entropic driving force for complex formation. Anion selectivity by BPTL²⁺ is governed by a synergistic interplay of electrostatic attraction, hydrogen bonding, and shape and size complementarity between the anion and the receptor's binding cavity. These insights offer valuable design principles for the next generation of hydrogen bonding receptors capable of functioning effectively in aqueous environments.

Experimental Section

Synthesis of tetralactam macrocycle 3: Benzene-1,2-diamine 2 (0.5 g, 4.6 mmol), TBACl (0.6 g, 2.3 mmol), and Et₃N (1.0 mL, 6.9 mmol) were dissolved in anhydrous CH₂Cl₂ (35 mL). Pyridine-3,5-dicarbonyl dichloride 1 (0.9 g, 4.6 mmol) was dissolved in anhydrous

CH₂Cl₂ (10 mL) and added dropwise to the reaction mixture over 1 minute under an ice bath. After stirring the reaction mixture for 10 minutes, the reaction was stopped, and the solvent was removed via vacuum. The resulting residue was washed six times with water (30 mL) to remove residual Et₃N and TBACl. The crude solid was then combined with TBACl (0.5 g) and dissolved in boiling ethyl acetate (500 mL). This mixture was allowed to cool to room temperature, and the resulting solid was removed by filtration. The filtrate was concentrated under reduced pressure, and the residue was washed with water to remove TBACl. This process (adding a small amount of TBACl, dissolving in boiling ethyl acetate, filtering, and washing) was repeated several times, each time using a slightly smaller quantity of TBACl until the ¹H NMR spectrum of the filtrate showed only the desired product (0.4 g, 57% yield). ¹H NMR (600 MHz, DMSO-d₆) δ 10.28 (s, 4H), 9.25 (d, *J* = 2.0 Hz, 4H), 9.04 (s, 2H), 7.94 (dd, *J* = 6.0, 3.6 Hz, 4H), 7.37 (dd, *J* = 6.1, 3.5 Hz, 4H). ¹³C NMR (101 MHz, DMSO-d₆) δ 163.8, 151.1, 134.6, 130.4, 129.8, 125.9, 125.3. HRMS(ESI) *m/z*: [M + H]⁺ Calcd for [C₂₆H₁₉N₆O₄]⁺: 479.1463 found: 479.1469.

Synthesis of BPTL²⁺·2Cl⁻: Macrocycle 3 (0.4 g, 0.8 mmol) was dissolved in DMF (5 mL), and iodomethane (1.0 mL, 16 mmol) was added. The mixture was stirred and heated at 100 °C overnight. After cooling to room temperature, the solvent was removed under reduced pressure, yielding a brown solid (BPTL²⁺·2I⁻). This solid was redissolved in DMF (5 mL), followed by the addition of KPF₆ (1.0 g, 5.4 mmol). Water (50 mL) was then added to induce precipitation of the intermediate salt, BPTL²⁺·2PF₆⁻. The precipitate was isolated by centrifugation, decanted, and thoroughly dried before being redissolved in MeCN (10 mL). TBACl (1.0 g, 3.6 mmol) was added, triggering precipitation of BPTL²⁺·2Cl⁻. The final product was collected by filtration, washed with MeCN, and dried to yield a white solid (0.2 g, 41% yield). ¹H NMR (600 MHz, D₂O) δ 9.59 (s, 4H), 9.36 (s, 2H), 7.87 (dd, *J* = 6.0, 3.5 Hz, 4H), 7.58 (dd, *J* = 6.0, 3.5 Hz, 4H), 4.63 (s, 6H). ¹³C NMR (101 MHz, DMSO) δ 160.8, 147.8, 141.7, 133.1, 129.9, 126.7, 125.7. HRMS(ESI) *m/z*: [M-2Cl⁻]²⁺ Calcd for [C₂₈H₂₄N₆O₄]²⁺: 254.0924 found: 254.0916.

The data that support the findings of this study are available in the [Supporting Information](#) of this article.

Acknowledgements

The National Science Foundation (CHE-2337419) and the University of South Florida start-up funding provided financial support for this work. This research used the X-ray and CPAS Core facilities at the University of South Florida, which were partly supported by the computational resources provided by the CIRCE research cluster facility.

Conflict of Interests

The authors declare no conflict of interest.

Data Availability Statement

Deposition Number(s) [2442988](#) and [2442989](#) contain(s) the supplementary crystallographic data for this paper. These data are provided free of charge by the joint Cambridge Crystallographic Data Centre and Fachinformationszentrum Karlsruhe Access Structures service.

Keywords: anions · hydrogen bond · molecular recognition · supramolecular chemistry · water

- [1] S. Kubik, *Chem. Soc. Rev.* **2010**, *39*, 3648.
- [2] M. J. Langton, C. J. Serpell, P. D. Beer, *Angew. Chem. Int. Ed.* **2016**, *55*, 1974.
- [3] J. Murray, K. Kim, T. Ogoshi, W. Yao, B. C. Gibb, *Chem. Soc. Rev.* **2017**, *46*, 2479.
- [4] J. Hatai, C. Schmuck, *Acc. Chem. Res.* **2019**, *52*, 1709.
- [5] A. P. Davis, *Chem. Soc. Rev.* **2020**, *49*, 2531.
- [6] J. Dong, A. P. Davis, *Angew. Chem. Int. Ed.* **2021**, *60*, 8035.
- [7] L. Escobar, P. Ballester, *Chem. Rev.* **2021**, *121*, 2445.
- [8] S. Kubik, *ChemistryOpen* **2022**, *11*, e202200028.
- [9] C. Zhai, A. Mariscal, W. Liu, *Trends in Chemistry* **2025**, *7*, 70.
- [10] X. Yang, W. Jiang, *J. Am. Chem. Soc.* **2024**, *146*, 3900.
- [11] R. A. Tromans, S. K. Samanta, A. M. Chapman, A. P. Davis, *Chem. Sci.* **2020**, *11*, 3223.
- [12] J. Samanta, M. Tang, M. Zhang, R. P. Hughes, R. J. Staples, C. Ke, *J. Am. Chem. Soc.* **2023**, *145*, 21723.
- [13] J. D. Einkauf, N. J. Williams, C. A. Seipp, R. Custelcean, *JACS Au* **2023**, *3*, 879.
- [14] A. E. Hargrove, S. Nieto, T. Zhang, J. L. Sessler, E. V. Anslyn, *Chem. Rev.* **2011**, *111*, 6603.
- [15] R. A. Tromans, T. S. Carter, L. Chabanne, M. P. Crump, H. Li, J. V. Matlock, M. G. Orchard, A. P. Davis, *Nat. Chem.* **2019**, *11*, 52.
- [16] M. V. Ramakrishnam Raju, S. M. Harris, V. C. Pierre, *Chem. Soc. Rev.* **2020**, *49*, 1090.
- [17] M. Zangiabadi, A. Ghosh, Y. Zhao, *ACS Nano* **2023**, *17*, 4764.
- [18] S. E. Border, R. Z. Pavlović, L. Zhiquan, J. D. Badjić, *J. Am. Chem. Soc.* **2017**, *139*, 18496.
- [19] C.-L. Deng, S. L. Murkli, L. D. Isaacs, *Chem. Soc. Rev.* **2020**, *49*, 7516.
- [20] A. T. Brockett, W. Xue, D. King, C. L. Deng, C. Zhai, M. Shuster, S. Rastogi, V. Briken, M. R. Roesch, L. Isaacs, *Chem* **2023**, *9*, 881.
- [21] C. J. Fowler, T. J. Haverlock, B. A. Moyer, J. A. Shriver, D. E. Gross, M. Marquez, J. L. Sessler, M. A. Hossain, K. Bowman-James, *J. Am. Chem. Soc.* **2008**, *130*, 14386.
- [22] R. Custelcean, N. J. Williams, C. A. Seipp, *Angew. Chem. Int. Ed.* **2015**, *54*, 10525.
- [23] S. K. Kim, J. Lee, N. J. Williams, V. M. Lynch, B. P. Hay, B. A. Moyer, J. L. Sessler, *J. Am. Chem. Soc.* **2014**, *136*, 15079.
- [24] M. Shmulevsky, X. Li, H. Shemer, D. Hasson, R. Semiat, *Journal of Membrane Science* **2017**, *524*, 299.
- [25] A. Chatla, I. W. Almanassra, A. Abushawish, T. Laoui, H. Alawadhi, M. A. Atieh, N. Ghaffour, *Desalination* **2023**, *558*, 116615.
- [26] L. Chen, S. N. Berry, X. Wu, E. N. W. Howe, P. A. Gale, *Chem* **2020**, *6*, 61.
- [27] R. Cao, R. B. Rossdeutcher, Y. Zhong, Y. Shen, D. P. Miller, T. A. Sobiech, X. Wu, L. S. Buitrago, K. Ramcharan, M. I. Gutay, M. F. Figueira, P. Luthra, E. Zurek, T. Szyperski, B. Button, Z. Shao, B. Gong, *Nat. Chem.* **2023**, *15*, 1559.
- [28] W. Zhao, A. H. Flood, N. G. White, *Chem. Soc. Rev.* **2020**, *49*, 7893.
- [29] C. R. Benson, L. Kacenauskaitė, K. L. VanDenburgh, W. Zhao, B. Qiao, T. Sadhukhan, M. Pink, J. Chen, S. Borgi, C. H. Chen, B. J. Davis, Y. C. Simon, K. Raghavachari, B. W. Laursen, A. H. Flood, *Chem* **2020**, *6*, 1978.
- [30] Y. Liu, W. Zhao, C.-H. Chen, A. H. Flood, *Science* **2019**, *365*, 159.
- [31] S. Lee, C. H. Chen, A. H. Flood, *Nat. Chem.* **2013**, *5*, 704.
- [32] A. P. Bisson, V. M. Lynch, M.-K. C. Monahan, E. V. Anslyn, *Angew. Chem. Int. Ed.* **1997**, *36*, 2340.
- [33] S. Wasiłek, J. Jurczak, *J. Org. Chem.* **2020**, *85*, 11902.
- [34] P. Niedbała, M. Majdecki, K. Dąbrowa, J. Jurczak, *J. Org. Chem.* **2020**, *85*, 5058.
- [35] Q. Q. Wang, V. W. Day, K. Bowman-James, *Angew. Chem. Int. Ed.* **2012**, *51*, 2119.
- [36] K. Bowman-James, *Acc. Chem. Res.* **2005**, *38*, 671.
- [37] M. M. Watt, L. N. Zakharov, M. M. Haley, D. W. Johnson, *Angew. Chem. Int. Ed.* **2013**, *52*, 10275.
- [38] S. C. Patrick, P. D. Beer, J. J. Davis, *Nat. Rev. Chem.* **2024**, *8*, 256.
- [39] L. P. Yang, X. Wang, H. Yao, W. Jiang, *Acc. Chem. Res.* **2020**, *53*, 198.
- [40] X. Huang, X. Wang, M. Quan, H. Yao, H. Ke, W. Jiang, *Angew. Chem. Int. Ed.* **2021**, *60*, 1929.
- [41] Y. Chen, G. Wu, L. Chen, L. Tong, Y. Lei, L. Shen, T. Jiao, H. Li, *Org. Lett.* **2020**, *22*, 4878.
- [42] X. Ren, A. J. Flint, D. Austin, A. P. Davis, *Angew. Chem. Int. Ed.* **2024**, *64*, e202413505.
- [43] S. Kubik, R. Kirchner, D. Nolting, J. Seidel, *J. Am. Chem. Soc.* **2002**, *124*, 12752.
- [44] L. Jing, E. Deplazes, J. K. Clegg, X. Wu, *Nat. Chem.* **2024**, *16*, 335.
- [45] É. M. Foyle, R. J. Goodwin, C. J. T. Cox, B. R. Smith, A. L. Colebatch, N. G. White, *J. Am. Chem. Soc.* **2024**, *146*, 27127.
- [46] C. Xu, Q. G. Tran, D. Liu, C. Zhai, L. Wojtas, W. Liu, *Chem. Sci.* **2024**, *15*, 16040.
- [47] M. J. Chmielewski, J. Jurczak, *Chem. Eur. J.* **2006**, *12*, 7652.
- [48] W. Liu, A. G. Oliver, B. D. Smith, *J. Org. Chem.* **2019**, *84*, 4050.
- [49] A. M. Gilchrist, D. A. McNaughton, M. Fares, X. Wu, B. A. Hawkins, S. J. Butler, D. E. Hibbs, P. A. Gale, *Chem* **2025**, *11*, 102329.
- [50] C. Zhai, C. Xu, Y. Cui, L. Wojtas, W. Liu, *Chem. Eur. J.* **2023**, *29*, e202300524.
- [51] C. Zhai, E. C. Zulueta, A. Mariscal, C. Xu, Y. Cui, X. Wang, H. Wu, C. Doan, L. Wojtas, H. Zhang, J. Cai, L. Ye, K. Wang, W. Liu, *Chem. Sci.* **2024**, *15*, 19588.
- [52] H. Pan, H. Huang, Y. Liu, J. Su, X.-K. Ren, Z. Chen, *Chem. Mater.* **2024**, *36*, 3745.
- [53] D. Brynn Hibbert, P. Thordarson, *Chem. Commun.* **2016**, *52*, 12792.
- [54] P. Thordarson, *Chem. Soc. Rev.* **2011**, *40*, 1305.
- [55] H. A. Fargher, L. H. Delmau, V. S. Bryantsev, M. M. Haley, D. W. Johnson, B. A. Moyer, *Chem. Sci.* **2024**, *15*, 5311.
- [56] A. J. Grooms, J. F. Neal, K. C. Ng, W. Zhao, A. H. Flood, H. C. Allen, *J. Phys. Chem. A* **2020**, *124*, 5621.
- [57] K. Dąbrowa, F. Ulatowski, D. Lichosyt, J. Jurczak, *Org. Biomol. Chem.* **2017**, *15*, 5927.
- [58] A. Docker, Y. C. Tse, H. M. Tay, A. J. Taylor, Z. Zhang, P. D. Beer, *Angew. Chem. Int. Ed.* **2022**, *61*, e202214523.
- [59] M. Berger, F. P. Schmidtchen, *Angew. Chem. Int. Ed.* **1998**, *37*, 2694.
- [60] R. Custelcean, N. J. Williams, C. A. Seipp, A. S. Ivanov, V. S. Bryantsev, *Chem. Eur. J.* **2016**, *22*, 1997.
- [61] P. Pracht, F. Bohle, S. Grimme, *Phys. Chem. Chem. Phys.* **2020**, *22*, 7169.
- [62] P. Pracht, S. Grimme, C. Bannwarth, F. Bohle, S. Ehlert, G. Feldmann, J. Gorges, M. Müller, T. Neudecker, C. Plett, S. Spicher, P. Steinbach, P. A. Wesolowski, F. Zeller, *J. Chem. Phys.* **2024**, *160*, 114110.
- [63] T. Lu, Q. Chen, *J. Comput. Chem.* **2022**, *43*, 539.
- [64] C. Lefebvre, G. Rubez, H. Khartabil, J.-C. Boisson, J. Contreras-García, E. Hénon, *Phys. Chem. Chem. Phys.* **2017**, *19*, 17928.
- [65] T. Lu, F. Chen, *J. Comput. Chem.* **2012**, *33*, 580.
- [66] T. Lu, F. Chen, *J. Theor. Comput. Chem.* **2012**, *11*, 163.
- [67] J. Zhang, T. Lu, *Phys. Chem. Chem. Phys.* **2021**, *23*, 20323.

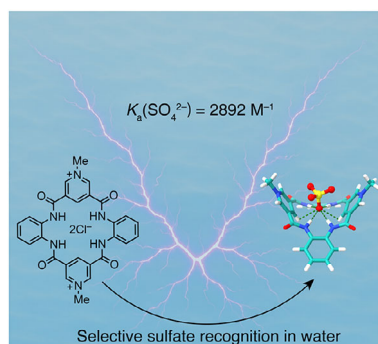
Manuscript received: April 11, 2025

Revised manuscript received: May 2, 2025

Version of record online: ■ ■ ■

RESEARCH ARTICLE

A dicationic tetralactam macrocycle achieves selective sulfate recognition in water via charge-assisted hydrogen bonding. Structural, thermodynamic, and computational studies reveal an entropy-driven mechanism enabled by electrostatic complementarity and desolvation. This work offers design principles for developing aqueous-phase receptors for sensing, separation, and catalysis.



A. Mariscal, L. Sagal, C. Doan, C. Zhai,
D. Liu, L. Wojtas, W. Liu

1 – 8

**Sulfate Recognition in Water via
Charge-Assisted Hydrogen Bonding**

